Mode Engineering in Large Arrays of Coupled Plasmonic–Dielectric Nanoantennas

Mazhar E. Nasir,* Alexey V. Krasavin, R. Margoth Córdova-Castro, Cillian P. T. McPolin, Jean-Sebastien G. Bouillard, Pan Wang, and Anatoly V. Zayats

Strong electromagnetic field confinement and enhancement can be readily achieved in plasmonic nanoantennas, however, this is considerably more difficult to realize over large areas, which is essential for many applications. Here, dispersion engineering in plasmonic metamaterials is applied to successfully develop and demonstrate a coupled array of plasmonic–dielectric nanoantennas offering an ultrahigh density of electromagnetic hot spots (10^{11} cm^{-2}) over macroscopic, centimeter scale areas. The hetero-metamaterial is formed by a highly ordered array of vertically standing plasmonic dipolar antennas with a ZnO gap and fabricated using a scalable electrodeposition technique. It supports a complex modal structure, including guided, surface and gap modes, which offers rich opportunities, frequently beyond the local effective medium theory, with optical properties that can be easily controlled and defined at the fabrication stage. This metamaterial platform can be used in a wide variety of applications, including hot-electron generation, nanoscale light sources, sensors, as well as nonlinear and memristive devices.

1. Introduction

Light can be efficiently localized at the nanoscale through the excitation of plasmonic modes supported by metallic nanostructures. The interaction of plasmonic modes in two or more metallic nanostructures separated by a nanoscale gap leads to even higher field localization and enhancement. The resulting intensity hot spots can be used for a variety of applications in field-enhanced nonlinear optical effects,[1–3] biochemical sensing,[4–6] as well as for the realization of localized light sources for imaging[6] and photocatalysis.[7] Nanoantennas of various geometries and shapes, including metallic strips,[8] bow-tie,[9] nanoparticle[10] and nano-disc[11] arrangements, core–shell nanostructures,[12] and nanorods,[13] have exhibited strong resonances and large field enhancement. The localized surface plasmons (LSPs) of metallic nanoparticles are the result of the coherent coupled oscillations of conduction electrons within the particle and the oscillations of the electromagnetic field within an optical mode tightly bound to it. The spectral positions and quality factors of the LSPs depend on the size, morphology, and materials of the particle, as well as the optical properties of the surrounding medium.[14] Furthermore, plasmonic nanostructures comprised of two or more material components present considerable advantages compared to commonly employed individual nanoparticles due to the additional degrees of freedom in their design, which vastly extend opportunities to engineer their optical properties to target particular applications.[7,12,15,16] Additionally, the corresponding near-field interaction between the plasmonic components strongly depends on the nanoparticle shape, relative position, gap size between adjacent nanoparticles and polarization of the excitation field.[15] Particularly, split metallic nanorods separated by nano-gaps show Fano resonances resulting from the interference of bright and dark modes in nanorod segments of various lengths. Therefore, such resonances can be tuned by changing the gap size and the lengths of the nanorod segments,[17] and have interesting applications in the fields of sensing and active plasmonic devices.

Metamaterials, composed of nanolayer composites or subwavelength arrays of nanoantennas (meta-atoms), have opened up a new era in optical materials, providing a revolutionary way to engineer the optical properties through nanostructuring. This led to the demonstration of several intriguing and practically important optical phenomena, such as negative index materials,[18] imaging beyond the diffraction limit,[19] optical cloaking[20] and giant nonlinearity.[21] Recently, a new class of metamaterials based on self-assembled arrays of ordered gold nanorods showed an exciting anisotropic optical behavior defined by the electromagnetic interaction between the rods

Dr. M. E. Nasir, Dr. A. V. Krasavin, Dr. R. M. Córdova-Castro,
Dr. C. P. T. McPolin, Prof. P. Wang, Prof. A. V. Zayats
Department of Physics and London Centre for Nanotechnology
King's College London
Strand, London WC2R 2LS, UK
E-mail: mazhar.nasir@kcl.ac.uk
Dr. J.-S. G. Bouillard
Department of Physics and Mathematics
University of Hull
Hull HU6 7RX, UK
Dr. J.-S. G. Bouillard
G. W. Gray Centre for Advanced Materials
University of Hull
Hull HU6 7RX, UK

in the array.[22,23] Due to the subwavelength inter-rod separation, their optical properties in the visible spectral range can be described within the effective medium theory (EMT) by a diagonal effective permittivity tensor $\varepsilon_{xx}^{\mathrm{eff}} = \varepsilon_{yy}^{\mathrm{eff}} \neq \varepsilon_{zz}^{\mathrm{eff}}$,[24] where the (x,y)-coordinate plane is perpendicular to the nanorod main axes and the z coordinate axis is along them. A particularly significant consequence of this is that above a certain wavelength in visible or near-IR regions $\varepsilon_{xx,yy}^{\mathrm{eff}} > 0$, while $\varepsilon_{zz}^{\mathrm{eff}} < 0$, which leads to striking changes in the optical behaviour of the metamaterial – its dispersion becomes hyperbolic.[25] Such metamaterials demonstrate many intriguing optical effects and a variety of possible applications in sensing and nanochemistry,[26–28] optomechanics,[29,30] neuromorphic computing,[31] emission control and lasing,[32–35] nonlinear optics,[36,37] and imaging.[38,39] Importantly, the optical response of a nanorod metamaterial layer, both in transmission and reflection, can be tuned throughout the visible and into the infrared spectral ranges by varying the geometry of the nanorod arrays and the permittivity of the surrounding medium at the fabrication stage[22,40,41] (see Figures S1–S3, Supporting Information). Particularly, template-based technologies offer a highly-controlled way to fabricate plasmonic nanostructures over large areas and in large quantities compared to conventional lithography and focused ion beam techniques.

In this study, we merge two major concepts of plasmonics: the ability of plasmonic structures to confine and enhance light at the nanoscale and engineering of the photonic modes in a complex metamaterial environment. This is achieved using a nanophotonic platform based on self-assembled Au/ZnO/Au split-rod metamaterials (**Figure 1**a,b). ZnO, which is a transparent and wide-bandgap semiconductor, forms a narrow gap between two gold segments, thus defining a nanoscale region for the strong field enhancement in the resulting split-rod nanoantenna, forming an elemental component of the metamaterial (meta-molecule). Furthermore, the resistance of ZnO gap material can be tuned from semiconductor to insulator at the fabrication stage during electrodeposition and post-treatment, which adds flexibility in the split-rod metamaterial design and the control of the resulting metamaterial optical properties. Experimental and numerical studies have revealed that the modal structure of a metamaterial layer in the visible spectral range is defined by a complex interaction of collective guided modes and localized modes supported by both the split-rod gap and the segments of plasmonic antennas themselves. For larger gap sizes, the optical response is mostly determined by the guided modes of the metamaterial heterostructure, which are modified by a phase delay introduced by the inter-rod dielectric layer. For smaller gaps (≈5 nm), however, a very pronounced new type of gap-mode of individual metamolecules is excited, which affects the optical response by interacting with the guided modes. Furthermore, they strongly localize the fields on the nanoscale and offer high intensity enhancement. In the mid-IR wavelength range, a previously overlooked surface mode guided by the metamaterial-air interface has been also observed. The
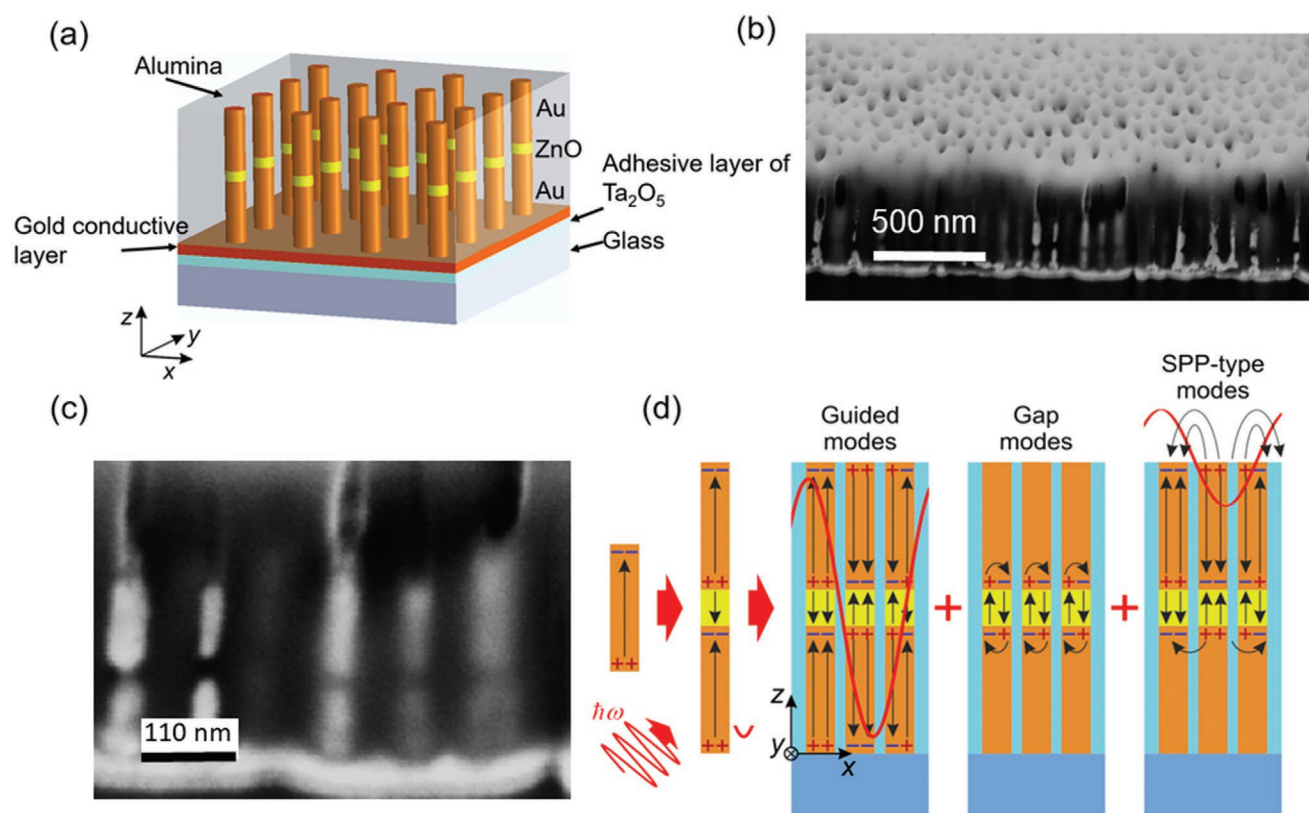
Figure 1. a) Schematic representation of the split-rod metamaterials. b) SEM cross sectional image of the split-rod metamaterial (Sample A). c) Zoom into the SEM image in (b). d) Sketch illustrating mode formation in an isolated nanoantenna and the split-rod metamaterial. Black arrows show the direction of the electric field, red curves signify the wave profile of the guided modes.

**ADVANCED
SCIENCE NEWS**

www.advancedsciencenews.com

**ADVANCED
OPTICAL
MATERIALS**

www.advopticalmat.de

presented approach provides a universal platform for realizing strong field enhancement on macroscopic scales in various settings and for a wide range of applications, such as photoluminescence and harmonic generation enhancement, control of hot-carrier dynamics and memristive behavior, as well as many others, utilizing a variety of plasmonic and dielectric materials.
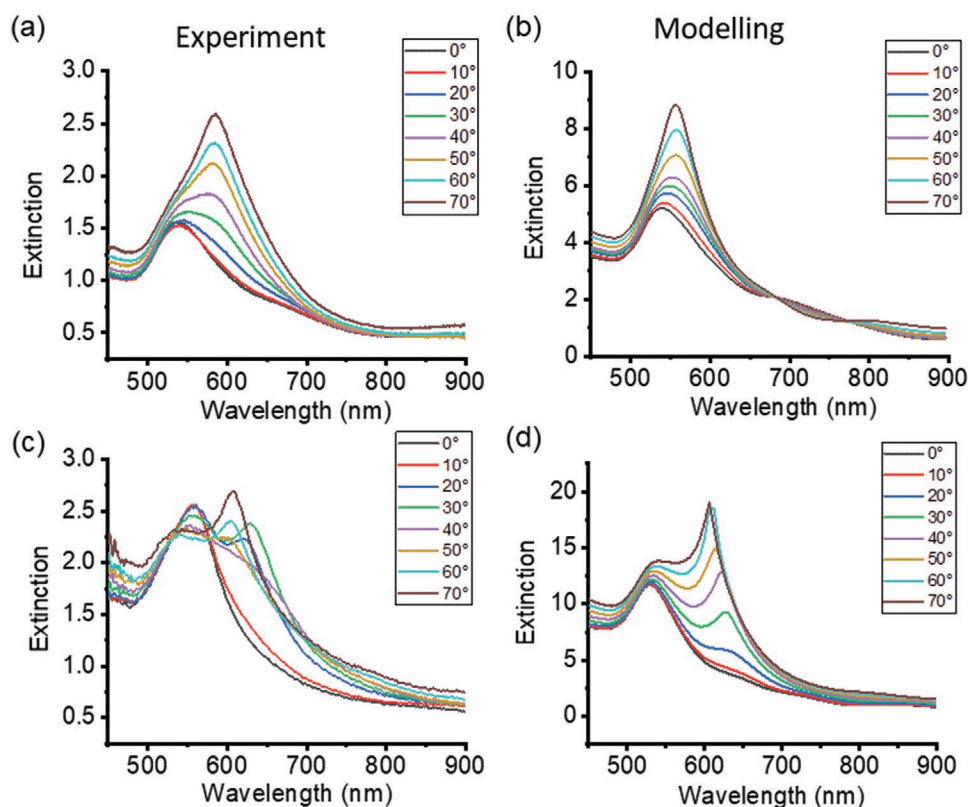
2. Results and Discussion

Split-rod metamaterials were fabricated via sequential electrodeposition of Au (bottom section), ZnO (middle section) and Au (top section) into a nanoporous Al_2O_3 (alumina, AAO) matrix produced by anodization of an Al film (see the Experimental Section). At the final step, they present a highly ordered subwavelength array of Au/ZnO/Au metamolecules comprised of two Au nanorod segments separated by a ZnO gap and embedded in an AAO matrix (Figure 1a–c). All geometrical parameters of the metamaterial can be easily controlled to engineer the optical response and to target particular applications. Two metamaterial samples with different parameters were fabricated and studied. In Sample A, both gold segments of the same size with a 56 nm diameter and a 100 nm length are separated by a 30 nm ZnO gap. In Sample B, the gold segments with a 50 nm diameter are unequal in length, being 200 and 450 nm long, and are separated by a 75 nm ZnO gap. In both samples the metamolecules form a quasi-periodic array with an average spacing of 100 nm. Within the framework of the local EMT theory, in the first approximation the optical properties of the nanorod metamaterial do not depend on the particular type of the nanorod arrangement, being defined only by the metal filling factor.[23,24,42] Both Au and ZnO are electrodeposited in a polycrystalline form.[42,43] Gold was chosen as a standard plasmonic material with relatively low losses, which assures high quality factors of the resonances and, therefore, high field enhancement. ZnO is a widely used material exhibiting photoluminescence, second-harmonic generation, and memristive behavior. Both plasmonic and dielectric components can be chosen from a wide variety of materials susceptible to electrodeposition. The employed nanostructuring process is based on self-organization and is fully scalable to the macroscale – the nanostructured areas of the studied samples have the size of ≈7 mm and can be extended further.

Generally, the optical behavior of the metamaterial heterostructure can be understood starting from the optical response of its individual meta-atoms (metallic nanorods) and their interaction with each other. A metallic nanorod supports a set of longitudinal plasmonic modes having different numbers of nodes along its length and generally a set of transverse modes (usually the dipolar mode vastly dominates). For example, the charge distribution corresponding to the fundamental longitudinal dipolar mode is shown in the left diagram in Figure 1d. When two nanorods are brought together, they become coupled and modes in the nanorods become hybridized. In the case of a tip-to-tip arrangement of nanorods, the hybridized mode with the lowest energy is presented in the diagram in Figure 1d. Being resonantly excited, this mode produces high field enhancement in the gap between the two nanorods, and, therefore, it is immensely beneficial to combine the nanoantennas in an array

and achieve a high density of the electromagnetic hot spots. When such a split-rod structure is placed in a closely spaced array with a subwavelength separation between the elements, there are effectively no diffractive effects and the nanostructure can be considered as a heterostructure of uniform uniaxial media each described by an effective permittivity tensor. The optical properties of such a heterostructure are defined by i) two absorption peaks in transmission and ii) resonant excitation of guided modes supported by the metamaterial. One absorption peak corresponds to the increased imaginary parts of the components ε_{xx}^{eff}, and ε_{yy}^{eff} descendent from the transverse dipolar plasmonic resonance of the individual nanorods, and the other is related to an epsilon-near-zero (ENZ) spectral range, marking an increase in the opacity/absorption when the effective permittivity component along the rods ε_{zz}^{eff} is close to zero.[42] The resonant excitation of the guided modes supported by the heterostructure can be clearly observed in reflection. There are three types of guided modes supported by this metamaterial (Figure 1d). The first type is a waveguided mode supported by the metamaterial layer, previously observed for conventional nanorod (no gap) metamaterials.[23] When a dielectric gap is introduced into the metamaterial layer, it produces a phase delay affecting the cross-sectional field distribution and, therefore, the properties of the guided modes. Additionally, due to the resulting capacitor-like charge distribution across the gap, substantial field enhancement in the gap can be achieved. In the case of narrow (≈5 nm) gaps, a new type of resonant plasmonic modes can be supported by the gap of the meta-atom, unique to the split-rod metamaterial. Finally, in the mid-infrared region, a surface mode supported by the metamaterial-air interface can be excited.

We start the experimental investigation with the study of the extinction properties of the heterostructure. In the case of p-polarized illumination, both split-rod metamaterials A and B exhibit two extinction peaks, with the magnitude of the long-wavelength peak increasing with the incident angle (**Figure 2**), reflecting the extinction properties of the conventional nanorod metamaterials at the top and at the bottom of the structure. The short-wavelength extinction peak, existing for both s and p polarizations of the incident light, corresponds to the absorption peak related to the excitation of the transverse plasmonic resonance of the gold nanorods (for both polarizations there is a field component across the nanorods). The long-wavelength peak, existing only for p polarization, is related to the wavelength at which the top and bottom metamaterial slabs are in the ENZ regime for the ε_{zz}^{eff} component. For s-polarization, it does not exist since there is no field along z-axis, while for p-polarization, its magnitude increases for larger angles with the increase of the electric field component in z-direction. The positions of the extinction peaks can be derived from the EMT and are defined by the metal filling factor.[23,24,42] In sample B, with a lower metal filling factor, the two peaks are well separated, as the position of the transverse nanorod resonance and the ε_{zz}^{eff} ENZ point are far apart (at 535 and 650 nm, respectively), while in sample A, with a higher metal filling factor, they spectrally overlap, when the transverse resonance position and the ENZ wavelength are separated by approximately a half of the resonance width (at 545 and 605 nm, respectively).

ADVANCED
SCIENCE NEWS
www.advancedsciencenews.com

ADVANCED
OPTICAL
MATERIALS
www.advopticalmat.de

Figure 2. Extinction spectra of the split-rod metamaterials. a,b) Sample A (symmetric 100 nm Au segments of a 55 nm diameter embedded in an AAO matrix and separated by a ZnO gap with a thickness of 30 nm) and c,d) Sample B (asymmetric 450 and 200 nm Au segments of a 50 nm diameter, embedded in an AAO matrix and separated by a ZnO gap with a thickness of 75 nm) at various angles of incidence: (a,c) experiment, (b,d) full wave numerical modelling. In both samples, the metamolecules are spaced in the array with a 100 nm period.
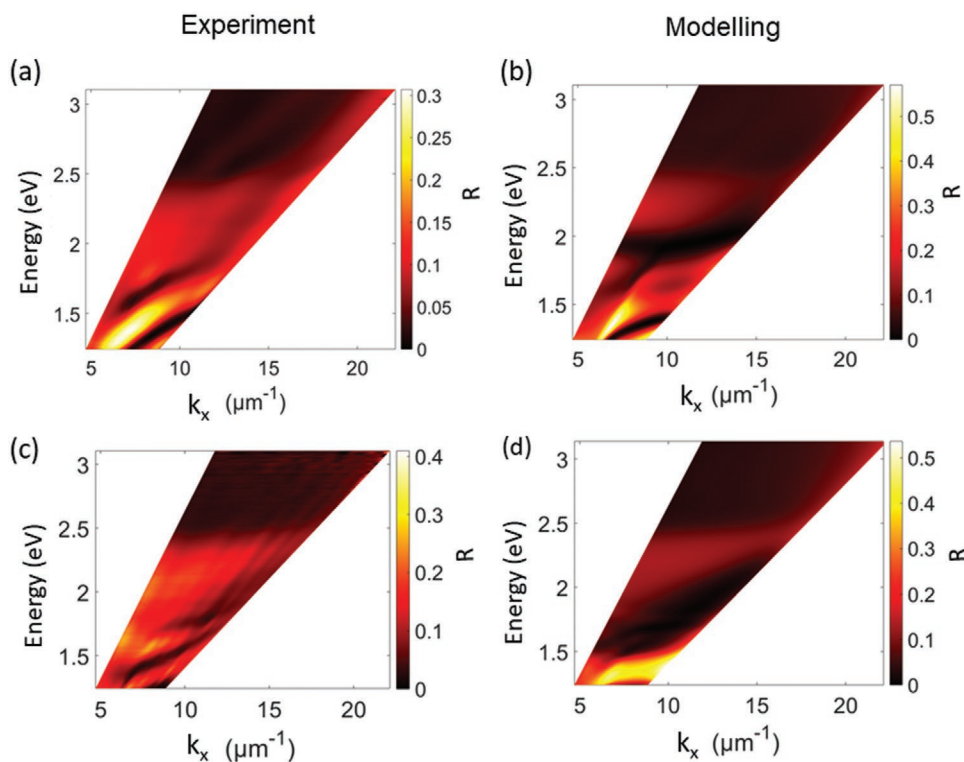
Moreover, the metamaterial layer supports waveguided modes,[23] which do not significantly contribute to the extinction due to the dominance of the above-described effects, but which can be clearly seen in reflection, particularly using an attenuated total reflection scheme. The measured modal dispersion, marked by dark regions in the angular spectra of reflectivity (**Figure 3**a,c), is in good agreement with the simulations (Figure 3b,d). Several guided modes of various orders can be identified by the minima in the reflection spectra (**Figure 4**). They can be easily traced to the original guided modes observed in the metamaterial layers without a gap (Figure S5, Supporting Information).[23] To get an insight into the physics of the guided mode formation, it is instructive to consider the EMT model, efficiently presenting it as a 3-layer heterostructure of uniform uniaxial metallic metamaterial slabs separated by a layer of its semiconductor counterpart. The spectral position and width of the fundamental guided mode in this case are predicted very precisely, while positions of higher-order resonances are spectrally shifted, as the EMT loses its accuracy toward shorter wavelengths (which start to be comparable with the nanorod spacing). It is interesting to note, however, that the intensity profiles across the layer are described by the EMT quite well.

To study the role of the gap width in the formation of the modes, the length of the metallic segments was fixed to 100 nm, while the thickness of the ZnO layer between them was varied from 20 to 100 nm. In this case, the mode spectral

positions move to longer wavelengths with the increase of the gap (Figure S6, Supporting Information). This evolution is particularly easy to understand for the fundamental mode which is well described by the EMT. With all components of the permittivity tensor of the metamaterial known, the system allows an analytical treatment as a 3-layer slab waveguide, upon which it was found that the observed spectral shift agrees with the analytical prediction with ≈10% precision. Thus, the guided nature of the observed modes is further confirmed by the analytical theory. The charge distribution at the tips of the gold segments forming the gap (Figure 4c) further confirms the general picture of the charge distribution for the guided modes: the modes of the 1st (at 904 nm) and 3rd (at 624 nm) order have modal local peaks in the middle of the structure and, therefore, an asymmetric charge distribution at the rod interfaces, while the mode of the 2nd order at 760 nm has a node there and, therefore, the corresponding symmetric charge distribution. As the guided modes propagate along the metamaterial layer, the field in the gap and the charge distribution at the nanorod/gap interfaces also move along the gaps in a wave-like fashion. It is interesting to note that a somewhat analogous approach involving a gradual change of the filling of the matrix has been used before, but for changing the position of the ENZ extinction peak.[44]

As in the case of close positioning of two individual plasmonic nanoparticles, a narrow gap between the nanorod

**ADVANCED
SCIENCE NEWS**
www.advancedsciencenews.com

**ADVANCED
OPTICAL
MATERIALS**
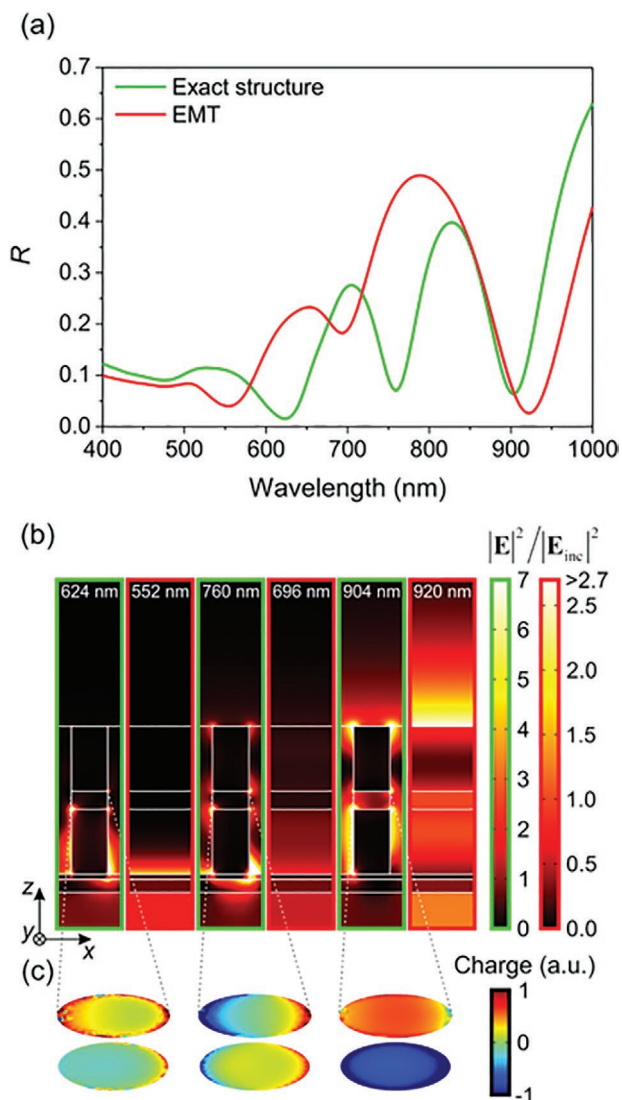www.advopticalmat.de

Experiment   Modelling

Figure 3. a,c) Experimentally measured and b,d) numerically simulated dispersion of the metamaterial modes determined using an attenuated total reflection with *p*-polarized light for samples (a,b) A and (c,d) B. The angular range corresponds to 30°–70° in glass.

segments of the split-rod metamaterial promises substantial enhancement of the local electromagnetic field intensity, leading to the increased light-matter interaction that is sought for numerous applications. Thus, nanorod materials with a 5 nm gap were studied, offering the prospect for the highest field enhancement in the region of validity of the applied theoretical framework (local material response and electromagnetic theory, not requiring quantum corrections). It was also assumed that the position of the gap across the metamaterial layer can affect the intensity enhancement, so it was varied, spanning the entire thickness of the metamaterial layer. Finally, the investigated spectral region was extended to include the full variety of the modes supported by the metamaterial layer (**Figure 5**). In the visible spectral range around 630, 740, and 870 nm, one can see the guided modes supported by the metamaterial layer identified above; their nature is also confirmed by the substantial field localization in the AAO matrix (Figure 5c,d). However, when the gap is close to the bottom ($z = 10$ nm) or is located in the region $z = 110–150$ nm, the position of the mode is pushed to lower wavelengths (Figure 5a,b), because the guided mode spectrally shifts simultaneously with the appearance of a completely new mode at a wavelength of 950 nm (seen for $z = 10, 100, 130, 160$ nm curves), demonstrating a classical modal anti-crossing behavior.

This mode is related to a substantial increase of the intensity in the gap region while it is extremely low in the surrounding matrix (Figure 5d). Thus, one can conclude that for the narrow gaps, a new type of mode exists in the visible spectral range, supported by the gap. Examining the electric field distribution inside the gap, one can see that it is a fundamental

metal-insulator-metal mode of the meta-atom, having two lobes in the electric field distribution (insets in Figure 5b).[33] It is interesting to note that, quite counterintuitively, although this type of mode is usually considered to be higher order (compared to the dipolar one), it is the fundamental gap mode in the considered system, as it is the lowest order mode possessing a feedback mechanism needed to produce a resonance. As can be expected, this mode can also be excited by the *s*-polarized illumination (see inset in Figure 5b). However, it can be excited only for certain positions of the gap in the metamaterial layer. Interestingly, in the EMT description (Figure S7, Supporting Information), this gap mode can be excited at all the gap positions. This leads to the conclusion that the EMT homogenization theory stops to be applicable in this case and the local modes supported by the metallic nanorods start to play a decisive role in the excitation of the gap mode. Similar effects have been observed in the detailed studies of the metamaterial layer extinction and fluorescence inside the metamaterial; this led to the extension of the local EMT theory with its nonlocal counterpart.[35,42]

There is yet another mode in the mid-IR region around 3000 nm which attracts attention. It cannot be either a guided mode or a gap mode, as it is located at a lower frequency compared to the fundamental modes of these types. It can be easily identified from its intensity distributions as a surface mode supported by the metamaterial-air interface (Figure 5c). Therefore, the metamaterial provides an opportunity to achieve surface mode guiding at the mid-IR spectral range where most plasmonic metals and highly doped semiconductors would fail. The mode exists both in the solid- and split-nanorod geometries. Coupling of this surface mode to the gap state provides

**ADVANCED
SCIENCE NEWS**

www.advancedsciencenews.com

**ADVANCED
OPTICAL
MATERIALS**

www.advopticalmat.de

Figure 4. a) Reflectivity of the split-rod metamaterial layer obtained using numerical modelling of the exact structure (green line) and the metamaterial heterostructure approximated using the EMT (red line). b) Electromagnetic field distributions in and around the metamaterial corresponding to the minima in (a) related to the mode excitation. c) Charge distributions at the top and bottom interfaces of the gap for the guided modes in the case of the discrete structure. The metamaterials parameters are as in Sample A, the *p*-polarized illuminating light is incident from the substrate side at the angle of 70°.

an opportunity for selective excitation of the gap mode at a different depth with a different illumination wavelength.

The enhancement of the local field intensity is extremely important for the increase of light-matter interactions. These phenomena are particularly interesting if they can be arranged in a controlled way in certain spatial regions. In this respect, the intensity hot spots present in the gap, and their relation to the modes supported by the metamaterial structure, are especially interesting. To study this aspect and reveal the optimal conditions for maximal field intensity enhancement, the ratio of the field intensities integrated over the gap volume and over the matrix domain was plotted as a function of the wavelength

and the gap position (**Figure 6**a), together with the electric field intensity profiles corresponding to the most efficient design-wavelength combinations (Figure 6b). In these simulations, the width of the gap was kept at 5 nm, as it offers the highest field enhancement in the region of applicability of the local electromagnetic theory and absence of the electron tunneling effects. The hot-spots, presented in two left profiles in Figure 6b, correspond to the excitation of the guided modes producing a capacitor-like charge/field distribution in the gap (as shown in Figures 1d and 4b,c), expectantly leading to the field enhancement, though with a moderate magnitude. The second region of the field enhancement, not visible in the ratio plot in Figure 6a, but giving the absolute maximum value of overall integral intensity in the gap (Figure 5e), is quite surprisingly related to the excitation of the surface waves at the metamaterial-air interface. As can be seen, the associated field, exponentially decaying into the metamaterial, can efficiently couple to the gap region. Very counterintuitively, the highest field intensity is not observed for the gap position close to the mode-supporting interface (where it is actually minimal), but closer to the opposite side (Figure 5e). This can be explained by the peculiarity of coupling- and distance-related phase shift between the incident light and the excited surface wave, influenced by the local phase response of the involved metallic segments. The absence of the corresponding local maximum in the ratio plot in Figure 6a confirms the essential delocalization of the mode, when, in addition to the hot spot, there is substantial presence of the mode fields in the matrix (Figure 6b, right intensity map), and in the air (Figure 5c). On the other side, the highest absolute and relative, with respect to the matrix, local field intensity is obtained with the quadrupolar gap modes (at 960 and 968 nm in Figure 6b). As discussed above (discussion of Figure 5e in relation to Figure S7, Supporting Information), the local field intensity has a prominent dependence on the position of the gap due to the structure of the modes supported by the individual metallic segments, which is not described by the local EMT theory.

3. Conclusions

We have developed a controllable and scalable technique to fabricate split-rod metamaterials produced by quasiperiodic arrays of metallic nanorods possessing a gap. All geometrical parameters of the metamaterials can be controlled at the fabrication stage, which, through the application of the design rules discussed above, gives the opportunity to engineer the modal structure and the local field enhancement. Particularly, in addition to the guided modes descendent from that in the nanorod metamaterials without a gap, a new type of metamaterial mode was revealed, specifically related to the resonant excitation in the semiconductor (or dielectric) gap, as well as a surface mode in the mid-IR spectral range. Generally, the surface mode gives the highest integral value of the electric field intensity in the gap, though with a substantial presence of the fields in the surrounding areas. On the contrary, the gap mode produces the field hot-spots with the highest intensity, strongly localized in the gap region. Engineering plasmonic modes in the developed metamaterial approach presents an easy, scalable and
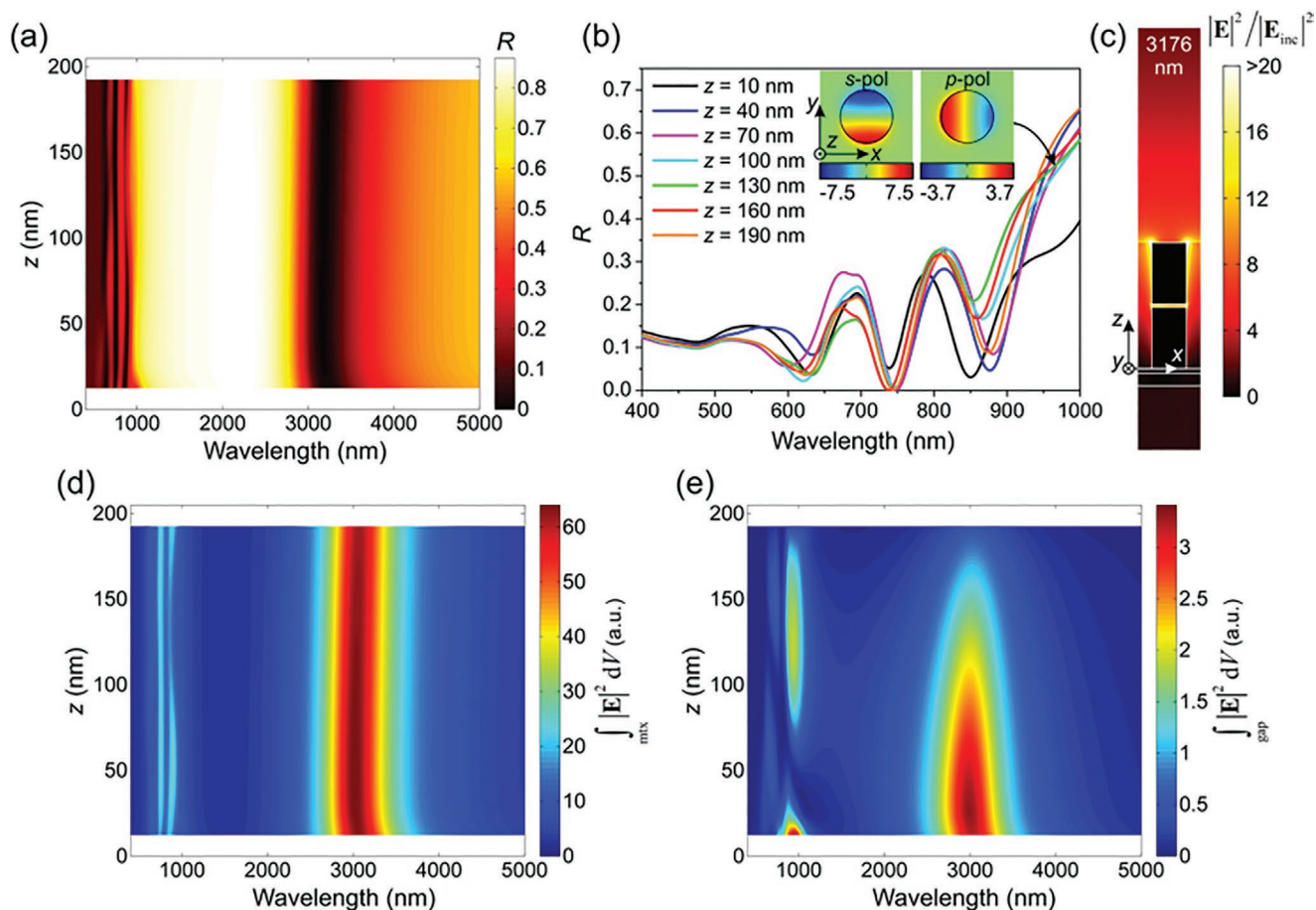
Figure 5. a) Reflectivity of *p*-polarized light incident on the split-rod metamaterial layer at 70° obtained using numerical modelling, as a function of the position of the 5 nm ZnO gap across the metamaterial thickness (for the reference coordinate system see (c)). b) Zoomed cross-sections of (a) for selected gap positions. The insets show E_z field distributions at the mid-height of the gap for the cases of the most efficient quadrupole gap mode in (b) for *s*-polarization ($z = 62.5$ nm, $\lambda = 952$ nm) and, *p*-polarization ($z = 132.5$ nm, $\lambda = 968$ nm). c) Electric field intensity profile of the surface mode at $\lambda = 3175$ nm. d,e) Distributions of the electric field intensity integrated over (d) the matrix and (e) the gap volume.
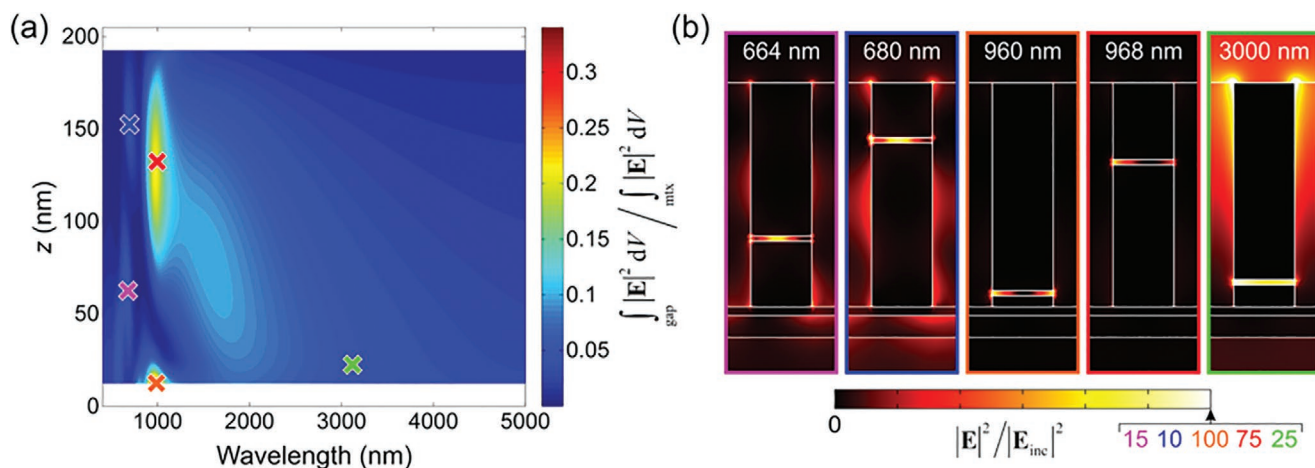
Figure 6. a) Ratio of the electric field intensities integrated over the gap volume (presented in Figure 5e) and the matrix domain (presented in Figure 5d) as a function of the wavelength and the position of the 5 nm ZnO gap across the metamaterial thickness, obtained using numerical modelling for *p*-polarized light incident on the split-rod metamaterial layer at 70°. b) The distributions of the electric field intensity for the modes corresponding to the local maxima in (a) as well as the absolute maximum in Figure 5e. The colors of frames around field maps in (b) correspond to the colors of the crosses in (a).

inexpensive platform for the realization of high-intensity hot spot arrays with a density exceeding 10^{11} cm^{-2}, which is important for many field-sensitive applications such as photoluminescence, hot carrier related phenomena and harmonic generation enhancement, or control of conductive filament formation in ultrahigh density memristive applications[31,45] when appropriately chosen material is deposited in the gap. A variety of active materials, such as polymers, other metals, ferromagnetic materials or indeed semiconductors, can be electrodeposited in the gap during fabrication. Therefore, the proposed architecture is an universal platform for realizing strong field enhancement in a wide range of settings and for a plethora of applications.

4. Experimental Section

Fabrication: The fabricated split-rod metamaterials consist of two Au segments separated by ZnO, electrochemically grown into ordered nanoporous alumina templates synthesized by a two-step anodization process (Figure S1, Supporting Information). An aluminum film with a thickness of 800 nm was sputtered on a substrate comprised of a glass slide covered with a 10 nm thick adhesion layer of tantalum pentoxide and a 7 nm thick Au film acting as an electrodeposition electrode. Tantalum pentoxide was deposited by sputtering tantalum in a 20% oxygen/ 80% argon atmosphere. Then, the aluminum was anodized in two steps using a 0.3 M oxalic acid solution at 3 °C and 40 V. The first anodization was carried out for 5 min. It produced a 200 nm thick alumina film with randomly oriented pores. After it, the porous oxide layer was completely etched in a mixed solution of H_3PO_4 (3.5%) and CrO_3 (20 g L^{-1}) at 70 °C leaving an ordered, patterned surface. The samples were then subjected to a second anodization step under the same conditions as in the first step to produce an alumina film with an array of highly ordered pores. They were subsequently etched in 30×10^{-3} M NaOH to remove a barrier layer at the bottom of the pores, thus exposing the gold electrode, and to tune the diameter of the pores. The pore geometry and spacing can be controlled over a wide range with nanoscale precision by the choice of the anodization conditions and chemical post-processing. The first electrodeposition of gold into the nanopores to produce the bottom metallic segment was performed in a three-electrode geometry using a non-cyanide solution. The electrochemical deposition of ZnO was carried out by the three-electrode system at −1.2 V using a bath containing 0.3 M Zn $(NO_3)_2$ and 0.1 M H_3BO_3 at 100 °C. After the short electrodeposition of ZnO on the top of the bottom gold segment, gold was electrodeposited again to produce the top gold segment. The length of the metallic segments was controlled by the electrodeposition time. Samples were annealed at 350 °C to tune the composition of ZnO. ZnO is one of the most commonly used transparent semiconductor oxides. It crystallizes in a wurtzite structure and has a direct wide band gap of about 3.4 eV at room temperature. The cathodoluminescence spectra and the EDX data of the samples confirm ZnO formation (Figure S4, Supporting Information).

Numerical Modelling: Numerical modelling was performed using a finite element method (COMSOL Multiphysics numerical simulation software). The model geometry is present in Figure S8 in the Supporting Information. The metamaterial was modelled as a square array of split-nanorod metamolecules, which gave the possibility to reduce the numerical complexity by considering a single unit cell setting proper Floquet boundary conditions on the cell sides, defined by the incident angle of the excitation wave. The top and bottom faces of the cell were equipped with perfectly matched layers (PMLs) to avoid back-reflections. The optical properties of gold were taken from tabulated experimental data[46] and corrected by setting the electron mean free path to 3 nm, which takes into account their variation due to the employed electrodeposition fabrication process. The data were extended into the mid-infrared spectral region applying a Drude-Lorentz model.[47] The optical properties of SiO_2 and Ti_2O_5 were taken

from Ref. [48,49] and Ref. [50] respectively, while Al_2O_3 was considered non-dispersive with the refractive index equal to 1.77. The effective medium simulations were performed using the model presenting the metamaterial as a 3-layer heterostructure of uniform uniaxial metamaterials with the optical axis directed perpendicular to the metamaterial plane. The optical properties of the layers were calculated using a local EMT.[23]

Supporting Information

Supporting Information is available from the Wiley Online Library or from the author.

Conflict of Interest

The authors declare no conflict of interest.

Data Availability Statement

The data that support the findings of this study are available from the corresponding author upon reasonable request.

[1] H. Linnenbank, Y. Grynko, J. Förstner, S. Linden, *Light: Sci. Appl.* **2016**, *5*, 16013.

[2] M. Kauranen, A. V. Zayats, *Nat. Photonics* **2012**, *6*, 737.

[3] A. V. Krasavin, P. Ginzburg, A. V. Zayats, *Laser Photonics Rev.* **2018**, *12*, 1700082.

[4] A. Kabashin, P. Evans, S. Pastkovsky, W. Hendren, G. Wurtz, R. Atkinson, R. Pollard, V. Podolskiy, A. V. Zayats, *Nat. Mater.* **2009**, *8*, 867.

[5] M. E. Nasir, W. Dickson, G. A. Wurtz, W. P. Wardley, A. V. Zayats, *Adv. Mater.* **2014**, *26*, 3532.

[6] T. Köker, N. Tang, C. Tian, W. Zhang, X. Wang, R. Martel, F. Pinaud, *Nat. Commun.* **2018**, *9*, 607.

[7] J. U. Salmón-Gamboa, M. Romero-Gómez, D. J. Roth, M. J. Barber, P. Wang, S. M. Fairclough, M. E. Nasir, A. V. Krasavin, W. Dickson, A. V. Zayats, *Faraday Discuss.* **2019**, *214*, 387.

[8] P. Muehlschlegel, H.-J. Eisler, O. J. Martin, B. Hecht, D. Pohl, *Science* **2005**, *308*, 1607.

[9] J. N. Farahani, D. W. Pohl, H.-J. Eisler, B. Hecht, *Phys. Rev. Lett.* **2005**, *95*, 017402.

[10] I. Romero, J. Aizpurua, G. W. Bryant, F. J. G. De Abajo, *Opt. Express* **2006**, *14*, 9988.

[11] P. K. Jain, M. A. El-Sayed, *Nano Lett.* **2007**, *7*, 2854.

[12] H. Wang, D. W. Brandl, P. Nordlander, N. J. Halas, *Acc. Chem. Res.* **2007**, *40*, 53.

[13] J. Dorfmüller, R. Vogelgesang, R. T. Weitz, C. Rockstuhl, C. Etrich, T. Pertsch, F. Lederer, K. Kern, *Nano Lett.* **2009**, *9*, 2372.

[14] W. L. Barnes, *Am. J. Phys.* **2016**, *84*, 593.

[15] P. K. Jain, M. A. El-Sayed, *Chem. Phys. Lett.* **2010**, *487*, 153.

**ADVANCED
SCIENCE NEWS**

www.advancedsciencenews.com

**ADVANCED
OPTICAL
MATERIALS**

www.advopticalmat.de

[16] P. Wang, A. V. Krasavin, F. N. Viscomi, A. M. Adawi, J. S. G. Bouillard, L. Zhang, D. J. Roth, L. Tong, A. V. Zayats, *Laser Photonics Rev.* **2018**, *12*, 1800179.

[17] Z.-J. Yang, Z.-H. Hao, H.-Q. Lin, Q.-Q. Wang, *Nanoscale* **2014**, *6*, 4985.

[18] S. Zhang, W. Fan, N. Panoiu, K. Malloy, R. Osgood, S. Brueck, *Phys. Rev. Lett.* **2005**, *95*, 137404.

[19] Z. Liu, H. Lee, Y. Xiong, C. Sun, X. Zhang, *Science* **2007**, *315*, 1686.

[20] W. Cai, U. K. Chettiar, A. V. Kildishev, V. M. Shalaev, *Nat. Photonics* **2007**, *1*, 224.

[21] J. Y. Ou, E. Plum, J. Zhang, N. I. Zheludev, *Adv. Mater.* **2016**, *28*, 729.

[22] M. Nasir, S. Peruch, N. Vasilantonakis, W. Wardley, W. Dickson, G. A. Wurtz, A. V. Zayats, *Appl. Phys. Lett.* **2015**, *107*, 121110.

[23] N. Vasilantonakis, M. E. Nasir, W. Dickson, G. A. Wurtz, A. V. Zayats, *Laser Photonics Rev.* **2015**, *9*, 345.

[24] J. Elser, R. Wangberg, V. A. Podolskiy, E. E. Narimanov, *Appl. Phys. Lett.* **2006**, *89*, 261102.

[25] A. Poddubny, I. Iorsh, P. Belov, Y. Kivshar, *Nat. Photonics* **2013**, *7*, 948.

[26] P. Wang, M. E. Nasir, A. V. Krasavin, W. Dickson, Y. Jiang, A. V. Zayats, *Acc. Chem. Res.* **2019**, *52*, 3018.

[27] V. V. Yakovlev, W. Dickson, A. Murphy, J. McPhillips, R. J. Pollard, V. A. Podolskiy, A. V. Zayats, *Adv. Mater.* **2013**, *25*, 2351.

[28] T. G. Mackay, *Opt. Eng.* **2015**, *54*, 067102.

[29] P. Ginzburg, A. V. Krasavin, A. N. Poddubny, P. A. Belov, Y. S. Kivshar, A. V. Zayats, *Phys. Rev. Lett.* **2013**, *111*, 036804.

[30] I. Nefedov, A. S. Shalin, *Phys. Status Solidi RRL* **2017**, *11*, 1700219.

[31] P. Wang, M. E. Nasir, A. V. Krasavin, W. Dickson, A. V. Zayats, *Nano Lett.* **2020**, *20*, 1536.

[32] L. Gu, J. Livenere, G. Zhu, T. Tumkur, H. Hu, C. Cortes, Z. Jacob, S. Prokes, M. Noginov, *Sci. Rep.* **2014**, *4*, 7327.

[33] R. Chandrasekar, Z. Wang, X. Meng, S. I. Azzam, M. Y. Shalaginov, A. Lagutchev, Y. L. Kim, A. Wei, A. V. Kildishev, A. Boltasseva, *ACS Photonics* **2017**, *4*, 674.

[34] D. J. Roth, A. V. Krasavin, A. Wade, W. Dickson, A. Murphy, S. P. Kéna-Cohen, R. Pollard, G. A. Wurtz, D. Richards, S. A. Maier, A. V. Zayats, *ACS Photonics* **2017**, *4*, 2513.

[35] P. Ginzburg, D. J. Roth, M. E. Nasir, P. Segovia, A. V. Krasavin, J. Levitt, L. M. Hirvonen, B. Wells, K. Suhling, D. Richards, A. V. Zayats, *Light: Sci. Appl.* **2017**, *6*, 16273.

[36] G. A. Wurtz, R. Pollard, W. Hendren, G. Wiederrecht, D. Gosztola, V. Podolskiy, A. V. Zayats, *Nat. Nanotechnol.* **2011**, *6*, 107.

[37] G. Marino, P. Segovia, A. V. Krasavin, P. Ginzburg, N. Olivier, G. A. Wurtz, A. V. Zayats, *Laser Photonics Rev.* **2018**, *12*, 1700189.

[38] J. Yao, K.-T. Tsai, Y. Wang, Z. Liu, G. Bartal, Y.-L. Wang, X. Zhang, *Opt. Express* **2009**, *17*, 22380.

[39] B. Casse, W. Lu, Y. Huang, E. Gultepe, L. Menon, S. Sridhar, *Appl. Phys. Lett.* **2010**, *96*, 023114.

[40] R. Starko-Bowes, J. Atkinson, W. Newman, H. Hu, T. Kallos, G. Palikaras, R. Fedosejevs, S. Pramanik, Z. Jacob, *J. Opt. Soc. Am. B* **2015**, *32*, 2074.

[41] R. Zang, H. Hu, X. Li, J. Gao, L. Liang, H. Zhang, F. Zhuge, J. Luo, H. Cao, *Opt. Lett.* **2019**, *44*, 2970.

[42] R. Pollard, A. Murphy, W. Hendren, P. Evans, R. Atkinson, G. A. Wurtz, A. V. Zayats, V. A. Podolskiy, *Phys. Rev. Lett.* **2009**, *102*, 127405.

[43] R. Inguanta, C. Garlisi, T. Spano, S. Piazza, C. Sunseri, *J. Appl. Electrochem.* **2013**, *43*, 199.

[44] W. Dickson, G. A. Wurtz, P. Evans, D. O'Connor, R. Atkinson, R. Pollard, A. V. Zayats, *Phys. Rev. B* **2007**, *76*, 115411.

[45] J. J. Yang, D. B. Strukov, D. R. Stewart, *Nat. Nanotechnol.* **2013**, *8*, 13.

[46] Y. Kurokawa, H. T. Miyazaki, *Phys. Rev. B* **2007**, *75*, 035411.

[47] P. B. Johnson, R. W. Christy, *Phys. Rev. B* **1972**, *6*, 4370.

[48] I. H. Malitson, *J. Opt. Soc. Am.* **1965**, *55*, 1205.

[49] C. Tan, *J. Non-Cryst. Solids* **1998**, *223*, 158.

[50] L. Gao, F. Lemarchand, M. Lequime, *Opt. Express* **2012**, *20*, 15734.